Soft Matter

PAPER

Cite this: *Soft Matter*, 2020, **16**, 411

Influence of the ion size on the stability of the smectic phase of ionic liquid crystals†

Wudi Cao,[ab] Beeran Senthilkumar,[c] Valerio Causin,[d] Vincent P. Swamy,*[c] Yanting Wang *[ab] and Giacomo Saielli *[de]

Received 24th October 2019,
Accepted 20th November 2019

DOI: 10.1039/c9sm02115a

rsc.li/soft-matter-journal

The thermotropic phase behavior of ionic liquids and ionic liquid crystals based on novel *N*-alkyl-3-methylpyridinium halides, trihalides and dichloroiodates was experimentally studied by polarized optical spectroscopy (POM) and differential scanning calorimetry (DSC) as well as by molecular dynamics (MD) simulation. In the experiments, the existence and thermal range of stability of the smectic phase of these ionic liquid crystals are found to strongly depend on the volume ratio between the cation and anion, that is their relative size. Only compounds with a relatively large volume ratio of the cation to anion, *i.e.*, those with longer cationic alkyl chains and monoatomic halide anions, have a stable smectic A phase. Both melting points and clearing points increase with such a ratio. The MD simulation results qualitatively agree very well with the experimental data and provide molecular details which can explain the experimentally observed phenomena: the stronger van der Waals interactions from the longer alkyl chains and the stronger electrostatic interactions from the smaller anions with a higher charge density increase the stability of both the crystal phase and the smectic phase; this also prevents the ionic layers from easily mixing with the hydrophobic regions, a mechanism that ultimately leads to a nano-segregated isotropic liquid phase.

Introduction

Ionic liquid crystals (ILCs) are compounds made of organic ions normally found in ionic liquids (ILs) and exhibiting a thermotropic liquid crystal (LC) behavior.[1] The constituent ions are usually imidazolium,[2–6] ammonium,[7] pyridinium,[8,9] bipyridinium,[10–16] and guanidinium[17–19] as the most common cations, and halides, BF_4^-, PF_6^-, and bis(trifluoromethanesulfonyl)imide (Tf_2N^-) as the most common anions. They are promising materials whenever mass and/or charge transport is sought in an ordered fashion, see for example recent applications as electrolytes in Li-ion batteries[20] and dye sensitized solar cells.[21,22] The reason behind the improved performance is facilitated ion transport in partially ordered, yet fluid, media.[23] For these reasons ILCs are attracting the attention of the materials science community.[24]

It is well known that within ILCs there is a scarcity of systems with a wide thermal range of the ionic nematic phase. With the exception of those reported in ref. 25, the existing ionic nematic systems are obtained by chemically linking a nematogenic core, such as cyanobiphenyl or cholesteryl groups, to an organic nitrogen salt.[7,26–28] Nonetheless, although classic DFT theory,[29] along with recent results based on MD simulations of mixtures of charged Gay–Berne and Lennard-Jones particles,[30–32] predicts the existence of the ionic nematic phase, the balance between electrostatic and anisotropic van der Waals (vdW) interactions needs to be carefully calibrated.

Common ILCs normally form smectic phases and the reason is easily understood: since the cations are made of an ionic head and one or more alkyl chains, nano-segregation of the polar network from the hydrophobic moieties leads to layered, that is smectic, phases with alternation of hydrophobic layers and ionic layers, akin to lamellar phases of lyotropic systems. In fact, mesomorphism appears only for chains longer than a minimum number of carbon atoms. If the carbon chain is below a certain limit, the systems only undergo a crystal-to-isotropic transition without any intermediate ILC phases. If we limit our discussion to a given family of compounds, *e.g.* 1-alkyl-3-methylimidazolium salts, [$C_nC_1$im][X], Nelyubina *et al.*[33] have

[a] *CAS Key Laboratory of Theoretical Physics, Institute of Theoretical Physics, Chinese Academy of Sciences, 55 East Zhongguancun Road, P. O. Box 2735, Beijing 100190, China. E-mail: wangyt@itp.ac.cn*
[b] *School of Physical Sciences, University of Chinese Academy of Sciences, 19A Yuquan Road, Beijing 100049, China*
[c] *Organic Chemistry Division, CSIR-National Chemical Laboratory, Dr Homi Bhabha Road, Pune 411008, India. E-mail: vp.swamy@ncl.res.in; Fax: +91 20 2590 2629; Tel: +91 20 2590 2313*
[d] *CNR Institute on Membrane Technology, Unit of Padova, Via Marzolo, 1 – 35131, Padova, Italy. E-mail: giacomo.saielli@unipd.it, giacomo.saielli@cnr.it*
[e] *Department of Chemical Sciences, University of Padova, Via Marzolo, 1 – 35131, Padova, Italy*

† Electronic supplementary information (ESI) available: Details of the synthesis and characterization. See DOI: 10.1039/c9sm02115a

shown that there is a linear correlation between the relative cation/anion volume and the existence of an ionic smectic phase. As the anion grows in size, the minimum number of carbon atoms necessary to have an ionic smectic phase also grows. For example, we have an ionic smectic phase for at least 10 carbon atoms in $[C_nC_1im][(FH)_2F]$,[34] while at least 22 carbon atoms are necessary to observe a smectic phase in $[C_nC_1im][TF_2N]$, which has a much larger anion. For a homologue series, *e.g.* the $[C_nC_1im]$ salts, an increased volume of the cation can only be obtained by an increase in the number of carbon atoms of the alkyl chain. Therefore, the relation between the volume of the cation and the volume of the anion can also be equivalently expressed as a relationship between the alkyl chain length of the cation and the volume of the anion.

Interestingly, the very same behaviour is observed for the "complementary" systems made of an anionic head linked to a variable alkyl chain paired with a metal cation, as is the case of metal alkanoates.[35–38] For example, in ref. 35 Mirnaya *et al.* reported that the liquid-crystalline state is not found in lithium alkanoates while it is present for alkyl chain lengths C_n with $n \geq 2$ for sodium salts, $n \geq 3$ for potassium salts, $n \geq 4$ for rubidium salts, and $n \geq 5$ for caesium salts. Therefore, also in this case, increasing the size of the counterion requires an increased chain length in order to observe an ionic LC phase, suggesting that the behaviour is very general and not related to the specific chemistry of the salts investigated.

Then the question is: why is a longer alkyl chain (of either imidazolium/pyridinium cations or alkanoate anions) needed to stabilize an ionic smectic phase with a larger counterion? To answer this question, it is useful to recall the structural features of an ionic smectic phase, as illustrated pictorially in Fig. 1 for the case of common imidazolium or pyridinium salts (the picture would be identical for metal alkanoates after switching the charges).

The key features of the bilayered smectic A (SmA) phase (usually found in ILCs) are (i) the arrangement of the molecules in alternating polar (cation heads and anions) and nonpolar alkyl chain layers; and (ii) the cylindrical symmetry around the phase director, and therefore an average orientation of the alkyl chains perpendicular to the layers. Despite the fact that the number density of atoms in the two layers does not have to be exactly the same, variations are expected within limited values in order to allow both cationic heads and anions, on the one hand, and alkyl chains, on the other hand, to completely fill the space. Alkyl chains can fill the space of the hydrophobic layer also by coiling and by interdigitation. This is the reason why the smectic periodicity is normally smaller than the full length of the cation.[39]

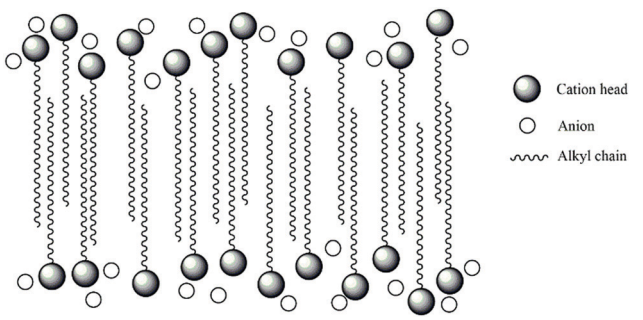

Fig. 1 Schematic representation of the structure of a bilayered SmA phase of a typical ionic liquid crystal. The straight arrangement of the alkyl chain is just a simplification to show the average orientation perpendicular to the smectic layers.

We can assume that the polar layer can be expanded by increasing the size of the anion, so in order to have a stable ionic smectic phase, longer chains are needed to fill the space of the hydrophobic layer (which must expand as well since the alkyl chains are covalently bonded to the cationic head groups). However, increasing the size of the anion has another effect: since the charge is normally $-1e$ (assuming the common halides BF_4^- or PF_6^- ILCs), a larger size of the anion necessarily means a lower charge density, leading to a reduced electrostatic interaction and a lower stability of the ionic layer.

To get more insight into the mechanism of stabilization of ionic smectic phases, we present here a combined experimental and molecular dynamics (MD) simulation investigation of the mesomorphic behavior of some new ILCs based on *N*-alkyl-3-methylpyridinium (C_nMP) halides, trihalides and dichloroiodates. The systems studied experimentally are $[C_nMP][X]$, with $X = Cl^-$, Br^-, I^-, Br_3^-, ICl_2^-, and I_3^- and $n = 12$, 14, and 16. For the MD simulations we selected a smaller subset, based on the experimentally observed phase behavior, with $n = 12$ and 16 and X = Br and Br_3^-. The analogous compounds with a short butyl chain, *N*-butyl-3-methylpyridinium halides and trihalides, had previously been studied and showed no liquid crystalline behavior.[40]

Results and discussion

Experimental

The thermal behavior of the synthesized materials has been characterized as described in the Experimental details section. The transition temperatures (with their transition enthalpies) and the phase assignments are reported in Table 1 and the thermal ranges of stability of the phases, with the corresponding enthalpies for melting into the isotropic phase (clearing point), are shown in Fig. 2. Selected POM micrographs are shown in Fig. 3 and 4, while selected DSC traces are shown in Fig. 5.

The various phases are assigned based on two pieces of experimental evidence: the enthalpy change, ΔH_c, at the clearing point, that is the transition from the ILC phase to the isotropic phase, and the textures observed on cooling from the melt under a microscope under polarized light. For the case of a liquid crystal–isotropic transition, ΔH_c should be relatively small, around 1 kJ mol^{-1} or less, and the textures should be consistent with a liquid crystal phase. In contrast, if either the enthalpy of transition is too high or the textures show typical spherulitic patterns indicating a crystal phase, or both, then the low temperature phase is assigned to be a crystal.

Table 1 Transition temperatures measured at the maximum of the DSC peak and the corresponding transition enthalpies in parenthesis

Compound	T/°C (ΔH/kJ mol^{-1})
[C_{12}MP][Cl]	Cr → 60.6 (7.4) → Iso
	Cr ← 34.7 (4.9) ← Iso
[C_{12}MP][Br]	Cr → 45.3 (0.6) → Iso
	Cr ← 14.8 (18.6) ← Iso
[C_{12}MP][I]	Cr → 16.4 (6.4) → Iso
	Cr ← −21.0 (1.4) ← Iso
[C_{12}MP][ICl_2]	Cr → 12.2 (6.3) → Iso
	Cr ← −40.0 (n.d.) ← Iso
[C_{12}MP][Br_3]	Cr → 24.0 (30.6) → Iso
	Cr ← −20.0 (1.3) ← Iso
[C_{12}MP][I_3]	Cr → 21.0 (39.9) → Iso
	Cr ← −23.0 (30.2) ← Iso
[C_{14}MP][Cl]	Cr → 99.5 (<0.1) → Iso
	Cr ← 61.2 (17.1) ← Sm ← 83.5 (0.1) ← Iso
[C_{14}MP][Br]	Cr → 81.0 (19.3) → Iso
	Cr ← 40.0 (24.4) ← Sm ← 68.0 (0.3) ← Iso
[C_{14}MP][I]	Cr → 47.3 (41.3) → Iso
	Cr ← 10.0 (19.2) ← Sm ← 35.2 (0.3) ← Iso
[C_{14}MP][ICl_2]	Cr → 29.4 (14.4) → Iso
	Cr ← 1.0 (22.5) ← Iso
[C_{14}MP][Br_3]	Cr → 74.1 (39.3) → Iso
	Cr ← 8.9 (16.1)← Iso
[C_{14}MP][I_3]	Cr → 33.6 (51.3) → Iso
	Cr ← 33.7 (50.3) ← Iso
[C_{16}MP][Cl]	Cr → 103.0 (26.6) → Sm →143.3 (0.6) → Iso
	Cr ← 61.4 (19.9) ← Sm ← 138.7 (0.7) ← Iso
[C_{16}MP][Br]	Cr → 84.6 (19.7) → Sm →131.1 (0.6) → Iso
	Cr ← 45.4 (26.3) ← Sm ← 128.0 (0.5) ← Iso
[C_{16}MP][I]	Cr → 63.8 (45.9) → Sm →116.2 (0.7) → Iso
	Cr ← 34.7 (35.6) ← Sm ← 111.7 (0.7) ← Iso
[C_{16}MP][ICl_2]	Cr → 50.0 (27.4) → Iso
	Cr ← 18.7 (14.9) ← Iso
[C_{16}MP][Br_3]	Cr → 78.0 (4.5) → Iso
	Cr ← 32.0 (19.1) ← Iso
[C_{16}MP][I_3]	Cr → 43.0 (57.3) → Iso
	Cr ← 32.0 (41.9) ← Iso

Based on this consideration we note that on cooling the samples after the first heating run the compounds with relatively long chains, [C_{14}MP]$^+$ and [C_{16}MP]$^+$, and relatively small anions ([Cl]$^-$, [Br]$^-$, and [I]$^-$) form a liquid crystal phase in a wide temperature range, which is wider and stable at higher temperatures for the [C_{16}MP][X] salts, compared to the analogous tetradecyl compounds. Some representative POM textures are shown in Fig. 3 and 4.

In Fig. 5 we show some representative DSC traces. We focus first on the two "opposite" samples [C_{12}MP][Br_3] in panel (b) and [C_{16}MP][Br] in panel (c) as representatives of a compound with a relatively small ratio between the cation and anion volume (the former one) and a compound with a relatively large ratio between the cation and anion volume (the latter one). It is clear that [C_{16}MP][Br] shows a typical pattern of an ionic liquid crystal phase between the low-enthalpy clearing-point peak of the transition from the smectic phase into the isotropic liquid and the high-enthalpy melting of the crystal into the smectic phase, see Table 1. In contrast, the DSC trace of [C_{12}MP][Br_3] shows a single high-enthalpy peak corresponding to the melting from the crystal into the isotropic liquid. The sample is then supercooled down to below 0 °C

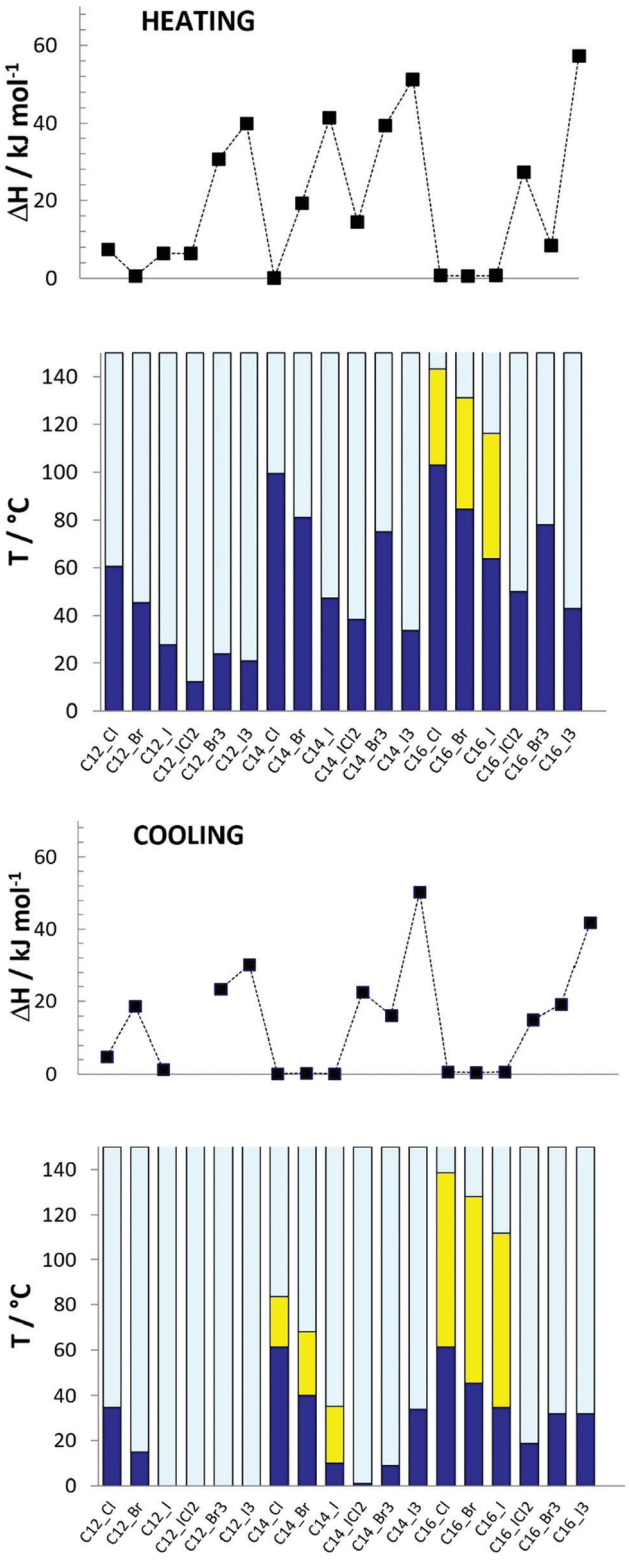

Fig. 2 Histograms of the thermal ranges of stability of the various 1-alkyl-3-methylpyridinium salts investigated: the (dark blue) solid; (yellow) smectic; and (light blue) isotropic phase. In the upper panels we report the enthalpies for melting into the isotropic phase. The label Cn_X represents the 1-alkyl-3-methylpyridinium with an alkyl chain length of n and the anion X (X = Cl^-, Br^-, I^-, ICl_2^-, Br_3^-, and I_3^-). The top two panels refer to the second heating run; the bottom two panels refer to the cooling run.

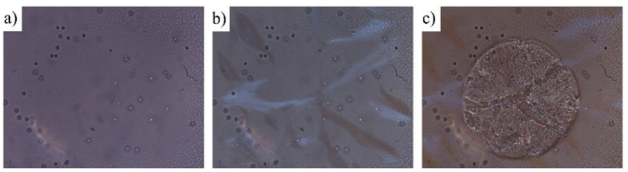

Fig. 3 Textures observed on cooling from the melt of the sample [C_{16}MP][Cl]. (a) T = 160 °C (isotropic phase); (b) T = 142 °C (marble textures indicating a smectic phase); and (c) T = 60 °C (spherulitic textures indicating a crystal phase).

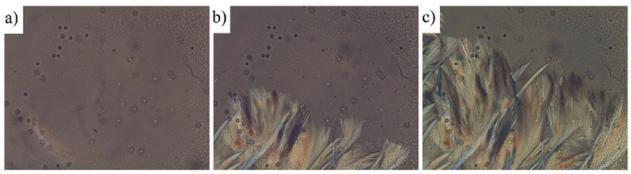

Fig. 4 Textures observed on cooling from the melt of the sample [C_{16}MP][ICl_2] at (a) T = 60 °C (isotropic phase); (b) T = 40 °C and (c) T = 35 °C. The slow growth of the spherulitic textures indicates a crystal phase.

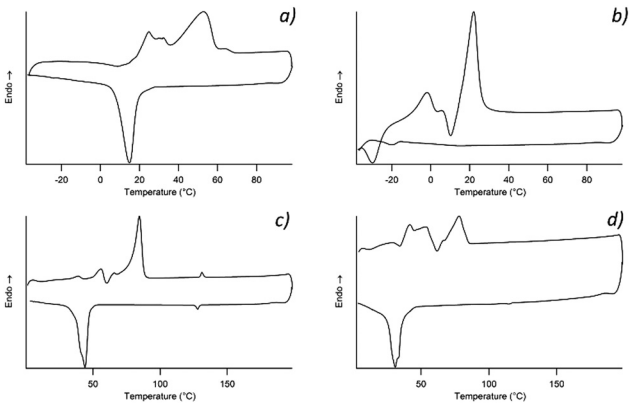

Fig. 5 DSC traces (second heating and cooling) of the samples: (a) [C_{12}MP][Br]; (b) [C_{12}MP][Br_3]; (c) [C_{16}MP][Br]; and (d) [C_{16}MP][Br_3].

with no evidence of any ionic mesophase. The other two samples, whose ratios between the cation volume and the anion volume are intermediate, also do not show any evidence of an ionic mesophase: the cooling run exhibits a single high-enthalpy peak, while the heating run shows a complex behavior due to possible crystal-to-crystal transitions. However, the final peak always has an associated relatively high enthalpy change, see Table 1 and Fig. 2.

There are some clear trends in the thermal behavior of the systems investigated. Considering all data in Table 1, we can say that the clearing point of the salts with a simple halide anion decreases regularly with increasing anion size in all cases. Replacing the simple monoatomic halide anions by the significantly larger polyatomic trihalide anions has a significant effect on the stability of the isotropic liquid phase: the clearing point is much lower and the intermediate ionic liquid crystal phase disappears. We do not observe any liquid crystal phase for the case of the $[C_{12}MP]^+$ series, and we obtain stable ionic liquids down to low temperatures below 0 °C for the ILs with larger anions. There is therefore a clear effect related to the relative cation/anion size, as described in ref. 33.

In order to shed light on this behavior, and gain microscopic insight into the mechanism behind the stabilization of the ionic smectic phase, we run all-atom MD simulations for the selected systems of [C_{12}MP][Br], [C_{12}MP][Br_3], [C_{16}MP][Br], and [C_{16}MP][Br_3].

Simulations

The simulated phase diagram of [C_{12}MP][Br], [C_{12}MP][Br_3], [C_{16}MP][Br], and [C_{16}MP][Br_3] is shown in Fig. 6. Specifically, [C_{12}MP][Br] melts at 505 K, when the crystal turns into a structure featuring rather ordered polar layers and disordered alkyl chains, which will be denoted by SmX. It is worth mentioning that the same arrangement, featuring an alternation of molten hydrophobic layers and ordered ionic layers, was proposed some years ago for an ordered smectic phase observed experimentally in dimeric viologen-based ionic liquid crystals.[12] The SmX phase observed in these simulations turns into a SmA ILC at 520 K when the ordered patterns within the polar layers disappear and the layer spacing increases. At 545 K, the SmA ILC finally undergoes a transition to an isotropic liquid phase characterized by a significant degree of nano-segregation, that is a nano-segregated liquid (NSL).[41,42] The details of the nano-segregation trend at the SmA–Iso transition in ILCs have also been studied in ref. 43. [C_{12}MP][Br_3] melts at 390 K directly into a NSL without going through the ILC phase. [C_{16}MP][Br] melts into a SmX phase at 515 K and then into SmA at 535 K. The SmA ILC ranges from 535 K to 685 K when the ILC becomes an isotropic NSL. [C_{16}MP][Br_3] melts into a SmA ILC at 450 K and then into a NSL at 465 K.

The order parameters, which quantitatively characterize the phases of the systems, are listed in Table 2, together with some other relevant structural and energetic data obtained from the simulations. Some representative snapshots of the structures are also shown in Fig. 7.

As found in our previous work,[44,45] the transition temperatures obtained from the simulations are much higher than those measured in experiments. However, this does not prevent

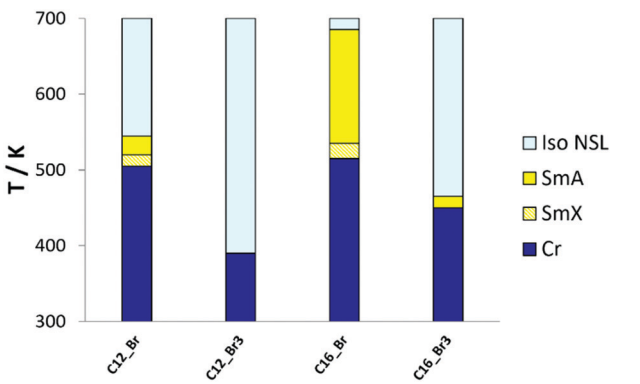

Fig. 6 Phase diagram of the four IL systems investigated by MD simulations.

Table 2 Layer spacing, order parameters, and Coulomb and van der Waals potential energy of the four systems investigated by MD simulations at temperatures featuring the various phases observed

	T, K	Structure	d, Å	τ_{LC}	S	E_{coul}, kJ mol^{-1}	E_{vdW}, kJ mol^{-1}
[C_{12}MP][Br]	515	SmX	18.43(9)	0.853(3)	0.53(1)	−278.3(3)	−79.7(5)
	520	SmA	29.5(3)	0.53(1)	0.31(1)	−274.4(4)	−77.9(4)
	545	Liquid	29.2(8)	0.22(2)	0.11(2)	−271.6(4)	−75.1(5)
[C_{12}MP][Br_3]	390	Crystal	29.29(7)	0.664(1)	0.949(3)	−196.5(2)	−133.3(4)
	390	Liquid	31.9(3)	0.217(6)	0.11(1)	−191.7(2)	−121.2(4)
[C_{16}MP][Br]	525	SmX	22.6(1)	0.892(7)	0.46(1)	−274.4(3)	−92.8(5)
	535	SmA	35.0(3)	0.76(1)	0.45(1)	−269.0(4)	−90.7(5)
	685	Liquid	—	0.11(2)	0.04(1)	−254.7(5)	−70.7(6)
[C_{16}MP][Br_3]	450	SmA	35.6(4)	0.46(1)	0.28(2)	−183.5(3)	−128.6(4)
	465	Liquid	—	0.14(2)	0.07(1)	−181.6(3)	−126.0(4)

us from qualitatively understanding the experimental data based on the simulation results since, although the absolute temperatures are incorrect, the relative trends still provide insightful information. We start our analysis by considering the melting points first: the melting points of the systems with the tribromide anion are lower than the corresponding transition temperature of the bromide salts, and for the compounds with the same anions, the melting points of the systems with the shorter chain (C_{12}) are lower than the corresponding transition temperature of the longer-chain system (C_{16}). This is indeed in agreement with our experimental findings.

Second, as far as the existence and thermal range of the ionic smectic phase are concerned, the [C_{12}MP][Br_3] system has no ILC phase, and the [C_{12}MP][Br] and [C_{16}MP][Br_3] systems have narrow ranges of ILC, which in addition features a smaller order parameter. In contrast, the [C_{16}MP][Br] system is the only one having a wide range of ILC with relatively large order parameters. These results too are in qualitative agreement with the experiments: a stable ionic smectic phase with a relatively large thermal range of stability is obtained only when we have a relatively large cation (long alkyl chain) along with a relatively small anion. Either decreasing the chain length (that is decreasing the cation volume) or increasing the anion volume leads to a significant destabilization of the ionic smectic phase.

The phase identification, according to the order parameters and visualization of the snapshots, is further confirmed by the radial distribution functions (RDFs) reported in Fig. 8. In particular, in Fig. 8(a) we show the anion–anion RDFs of [C_{16}MP][Br]. The crystal phase at 510 K is highly ordered, as suggested by the fine structure of the corresponding RDF, while such modulation is almost completely lost in the isotropic NSL at 685 K. The RDF for the ionic smectic phase at 600 K is also very close to the isotropic liquid, indicating a very similar local

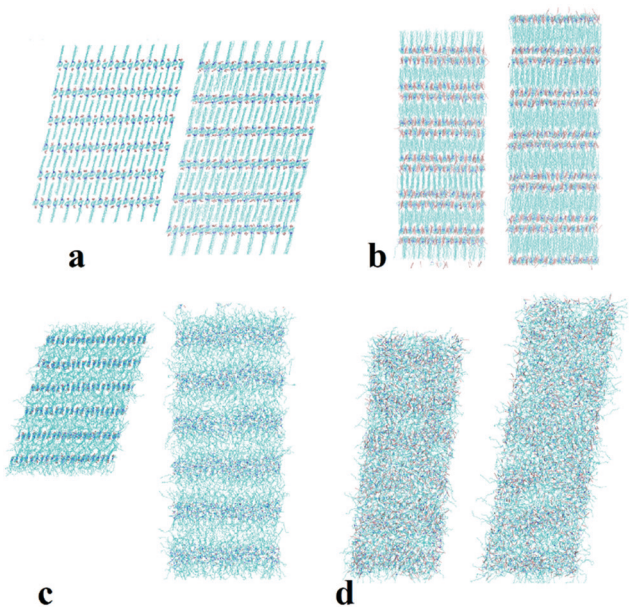

Fig. 7 Snapshots of (a) crystal structures of [C_{12}MP][Br] at 500 K and [C_{16}MP][Br] at 510 K; (b) crystal structures of [C_{12}MP][Br_3] and [C_{16}MP][Br_3] at 385 K and 445 K; (c) SmX structure of [C_{12}MP][Br] at 515 K and SmA structure of [C_{16}MP][Br] at 600 K; and (d) nano-segregated liquid structures of [C_{12}MP][Br_3] at 390 K and [C_{16}MP][Br_3] at 465 K.

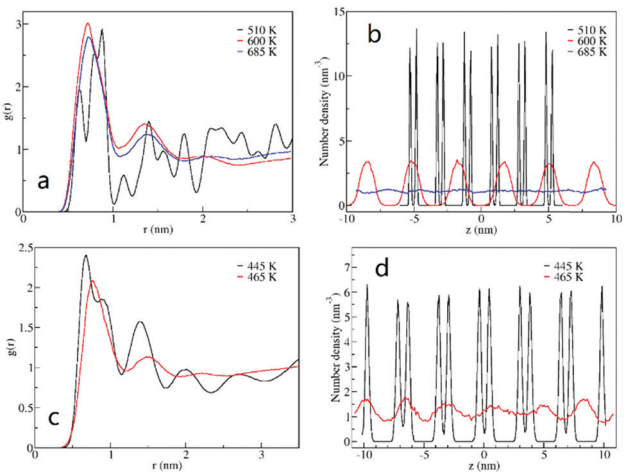

Fig. 8 (a) RDFs of Br–Br in [C_{16}MP][Br] at 510 K in the crystal phase (black), at 600 K in the LC phase (red) and at 685 K in the liquid phase (blue); (b) number densities of [Br] in [C_{16}MP][Br] along the z-axis at 510 K (black), 600 K (red), and 685 K (blue); (c) RDFs of Br2–Br2 (Br2 being the Br in the middle of [Br_3]) in [C_{16}MP] [Br_3] at 445 K in the crystal phase (black) and at 465 K in the liquid phase (red); and (d) number densities of Br2 in [C_{16}MP][Br_3] along the z-axis at 445 K (black) and 465 K (red).

environment.[43,46] The number density profile along the *z*-axis, shown in Fig. 8(b), is consistent with the RDF and with the long-range translational order in Table 2: a strongly peaked distribution is observed for the crystal phase at 510 K, while an almost flat line is found in the isotropic phase at 685 K, indicating a complete lack of translational order. However, a significantly modulated density profile is observed for the smectic phase at 600 K, without any additional fine structure of the peaks; this indicates alternation of layers without any additional structure within the layers, as expected for a smectic liquid crystal phase.

The analogous plots for the tribromide analogue, [C_{16}MP][Br_3], see Fig. 8(c and d), only show the presence of a crystal (445 K) and an isotropic NSL phase (465 K), despite the fact that residual weak modulation is observed in the latter case which disappears during further heating.

Therefore, we can propose a qualitative mechanism for ionic smectic phase stabilization/destabilization based on our simulation results. For the systems with the same anion but different alkyl-chain length *n*, the electrostatic interactions are similar in strength (see Table 2), while the vdW interaction between alkyl chains increases with *n*. These issues have already been discussed in detail in previous work[47] and explain the well-known trend in the melting and clearing points of imidazolium salts.[48] On the other hand, a higher charge density also contributes in the same direction to the stability of the smectic phase: MD simulations revealed a phase diagram as a function of the charge density having a little effect on the crystal-to-SmA transition temperature and a much more pronounced effect on the SmA–isotropic clearing point, which increased significantly upon increasing the charge density of the ionic parts.[49] On the opposite side, we can easily understand that by decreasing the chain length, and thus reducing the vdW interaction of the hydrophobic layer, and at the same time increasing the size of the anion, and thus reducing the electrostatic interaction of the ionic layer, the isotropic liquid is strongly favoured, whose stability can reach room temperature and below.

The appearance of a SmA phase is, therefore, due to a balance between these opposite trends. It is interesting to note that these effects finally find their balance on separate layers: we can ideally destabilize the ionic layers of an ionic SmA phase by increasing the size of the anions (thus, lowering the electrostatic interaction) and compensate this effect by stabilizing the hydrophobic layer *via* increasing the chain length (thus increasing the vdW interaction) in order to keep the ionic SmA phase over a range of temperatures. Moreover, the longer the alkyl-chain length, the thicker the alkyl chain regions. The transition enthalpy from the ILC to the NSL is much smaller than that from the crystal to the ILC. The main difference between the ILC and NSL is that the polar regions in the ILC form separated layers, while they are a connected network in the NSL (see Fig. 9). Therefore, the simulations also provide an insightful view on the mechanism of the transition and further support the arguments in favour of the energetic stabilization/destabilization of the ionic smectic phases. At the transition

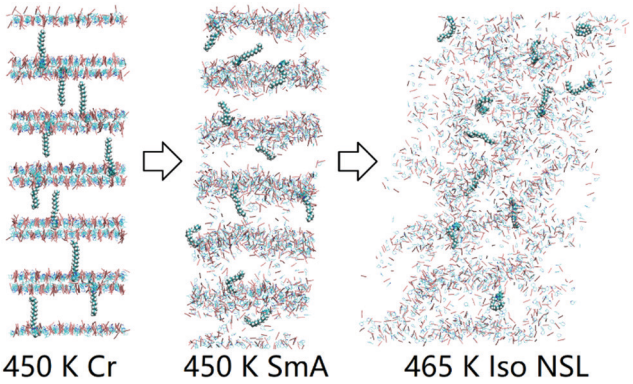

Fig. 9 Snapshots of [C_{16}MP][Br_3] at 450 K before and after the crystal–SmA ILC transition and at 465 K in the isotropic NSL phase, showing the polar sites "entering" the nonpolar alkyl-chain regions, which finally breaks the polar layer structure. This can be compared with Fig. 7(c), where the polar sites of [C_{16}MP][Br] stay in the polar layers even at 600 K.

from a SmA phase into an isotropic liquid, for the system with a longer *n*, the ionic sites at both sides of the nonpolar region must intrude deeper into the nonpolar region to be close enough to form the polar network. This requires a higher thermal energy, compared to a system with shorter chain length, and, therefore, it is the reason why the [C_{16}MP][Br] system has a large ILC thermal range but [C_{12}MP][Br] does not. In contrast, the lower charge density of tribromide anions allows them to enter the hydrophobic region in an easier way than the bromides and therefore the connected polar network characteristic of the isotropic NSL can be formed at lower temperatures, possibly even below the virtual SmA-to-isotropic transition. Consequently, [C_{12}MP][Br_3] shows no ILC phase and the ILC range of [C_{16}MP][Br_3] is only 15 K even at the simulation timescale.

The mechanism of the transition from the smectic phase into the isotropic nano-segregated liquid was investigated also in ref. 43 by using a coarse-grained version of the force field representing an imidazolium nitrate. We have found that a very useful parameter to follow the mechanism of the transition is the heterogeneity order parameter (HOP), $\langle h \rangle$, see the Computational section. This parameter measures the degree of homogeneity in the sample, that is the degree of nano-segregation of the alkyl parts from the ionic moieties. Interestingly, in ref. 43 the value of $\langle h \rangle$ was found to increase on cooling from the isotropic nano-segregated liquid into the ionic smectic phase, indicating a significant role of microphase segregation in stabilizing the layered phase.

Here we calculate the HOPs from the fully atomistic simulations of our systems in the various phases. The values are reported in Table 3.

It is clear from the values reported in Table 3 that the HOP increases on going from the isotropic nano-segregated liquid into the smectic phase for all sites selected, either representing the alkyl chains or the ionic parts. This result indicates closer contact and higher segregation of the alkyl chains from the ionic parts of the molecules. Therefore, the discussion above concerning the relative stability of the hydrophobic and ionic

Table 3 Heterogeneity order parameter, $\langle h \rangle$, from the fully atomistic simulations of the systems investigated in the various phases

	T/K	Phase	$\langle h \rangle$ head[a]	$\langle h \rangle$ tail[a]	$\langle h \rangle$ anion[a]
$[C_{12}MP][Br]$	515	SmX	0.43(2)	0.36(2)	0.32(2)
	520	SmA	2.81(8)	3.2(1)	2.25(6)
	545	NSL	2.3(1)	2.6(1)	1.9(1)
$[C_{12}MP][Br_3]$	390	Cr	3.01(2)	2.02(3)	2.13(2)
	390	NSL	1.57(3)	3.4(1)	1.20(2)
$[C_{16}MP][Br]$	525	SmX	1.17(3)	0.63(3)	0.97(2)
	535	SmA	5.5(2)	4.6(2)	4.7(1)
	685	NSL	3.2(1)	2.02(8)	2.7(1)
$[C_{16}MP][Br_3]$	450	SmA	3.3(1)	4.7(2)	2.71(9)
	465	NSL	2.65(7)	3.9(1)	2.20(6)

[a] ''head'' refers to the center of mass of the pyridinium ring, ''tail'' refers to the methyl terminal carbon of the alkyl chain and ''anion'' refers to the center of mass of the anion.

layers due to a separate effect of van der Waals and electrostatic interactions finds further support and justification in the high degree of segregation of the ionic smectic phase.

Experimental

Synthetic procedures

The compounds investigated have been synthesized according to the procedures in Scheme 1. A detailed description of the synthetic protocols and characterization of the compounds can be found in the ESI.†

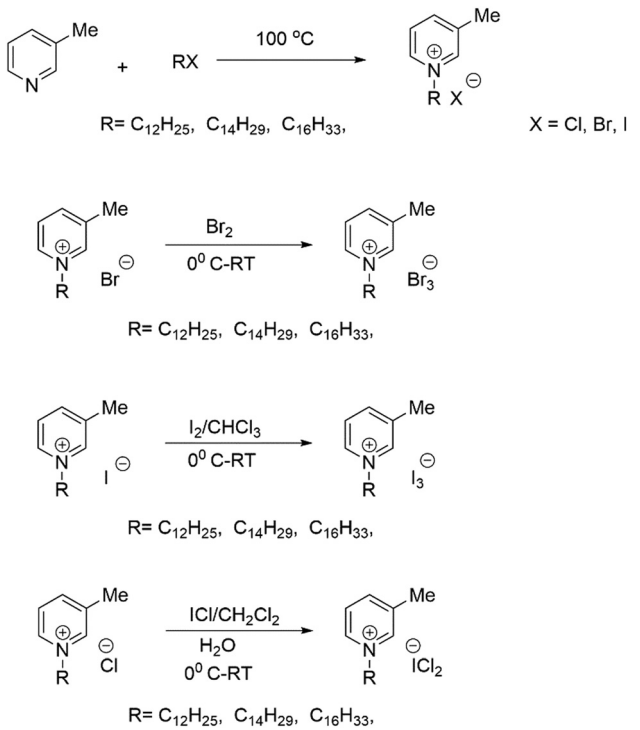

Scheme 1 Synthetic procedures of the compounds investigated.

Materials and methods

POM (Polarized Optical Microscopy). The textures of the samples were studied with a Leica DM4000M polarized light microscope. The samples were placed between a glass slide and a cover slip. A Mettler FP82HT hot stage was used to control the temperature. The samples were heated at 10 °C min^{-1} beyond the melting temperature determined by DSC experiments, and subsequently cooled at 10 °C min^{-1} to room temperature. The photomicrographs were taken between cross-polarizers with a Leica DFC280 digital camera.

DSC (differential scanning calorimetry). All the measurements were carried out with a TA Instruments mod. 2920 calorimeter operating under an N_2 atmosphere. Samples weighing about 5 mg closed in aluminum pans were used throughout the experiments. Indium of high purity was used for calibrating the DSC temperature and enthalpy scales. Four ramps were included in the temperature program: one heating from room temperature to 200 °C at 10 °C min^{-1}, followed by a cooling step to room temperature at 10 °C min^{-1} and by another analogous heating/cooling cycle. The repetition of two similar heating/cooling ramps was done to assess the repeatability of the phase transitions.

Simulation setup

We modeled the ILs using the GAFF (general Amber force field) scheme.[52] For the 1-dodecyl/hexadecyl-3-methylpyridinium [C_{12}/C_{16}MP] cation and the Br^- anion, the available force field parameters in GAFF were adopted. The tribromide Br_3^- anion is a resonance hybrid and since all bromine atoms have the same vdW parameters in GAFF, we adopted the parameters accordingly. The bond and angle parameters of Br_3^- are obtained by fitting the *ab initio* calculations at the MP2/6-31G* level, using the paramfit program provided in the AmberTools18 package.[53] The HF/6-31G* RESP charge method[54] was applied to determine the partial charges, and the Gaussian09 package[55] was used for the *ab initio* calculations. The obtained new parameters of the tribromide anion are set as follows: the partial charge of the two terminal Br atoms is −0.43716; the partial charge of the central Br atom is −0.12568; the Br–Br equilibrium bond distance is b_0 = 2.5779 Å; the harmonic stretching constant is K_b = 64.1488 kcal mol^{-1} $Å^{-2}$; the Br–Br–Br angle is $\theta_0 = 180°$ and the harmonic bending constant is K_θ = 37.4898 kcal mol^{-1} rad^{-2}.

The Parrinello–Rahman barostat[56] and the Nosé–Hoover thermostat[57] were applied to control the shape and size of the simulation box and the system temperature, respectively. The barostat was set to be anisotropic with all components of the reference pressure being 1 bar because we were simulating crystal and liquid crystal phases, both of which are anisotropic. Periodic boundary conditions (PBC) were applied in three dimensions and the electrostatic interactions were calculated with the Particle–Mesh Ewald (PME) method.[58] The real-space cutoff for PME and vdW interactions was set to 1.2 nm. The simulation trajectories were visualized by VMD software,[59] which was also used for constructing and modifying the initial crystal structures. The GROMACS package[60] was used to perform the MD simulations.

The initial crystal structures of [C_{16}MP]Br and [C_{16}MP][Br_3] were built starting from the structures reported in ref. 61 and 62 for *N*-tetradecylpyridinium bromide monohydrate and *N*-hexadecylpyridinium diiodochloride, respectively. The *N*-tetradecylpyridinium bromide monohydrate reported in ref. 61 was modified to *N*-hexadecyl-3-methylpyridinium bromide by removing the water molecule and adding a methyl group in position 3 of the ring and adding two more carbon groups in the chain. The *N*-hexadecylpyridinium diiodochloride reported in ref. 62 was modified to *N*-hexadecyl-3-methylpyridinium tribromide in a similar way. The structures of [C_{12}MP]Br and [C_{12}MP][Br_3] were obtained by truncating a C_4H_8 group on the cationic alkyl side chain. All the four structures were carefully refined by MD simulation. For each simulation, there are 1440 ion pairs in the simulation box.

The systems were heated stepwise and at each temperature the MD simulation time ranged from several nanoseconds to hundreds of nanoseconds, whose equilibration was verified by the time invariance of energy and the values of the order parameters including the orientational order parameter for cations and translational order parameters for polar sites, *i.e.*, the center-of-mass of the methylpyridinium rings and anions. The orientational order parameter S is defined as

$$S = \langle P_2(\cos\theta)\rangle \quad (1)$$

where P_2 is the second Legendre polynomial, and θ is the angle between the phase director and the directional vector of a cation pointing from the polar site to the tail group. The translational order parameter τ_{LC} is defined as

$$\tau_{LC} = \frac{1}{N_t}\left|\sum_{\alpha=0}^{N_t}\exp(iz^{\alpha}/d)\right| \quad (2)$$

where z^{α} is the z-component of the position with the index α representing all the polar sites including both head groups and anions, N_t is the total number of polar sites, and d is the smectic periodicity. More details about the calculation of both the orientational and translational order parameters can be found in our previous work[45] or the original paper.[63]

Finally, the homogeneity order parameter, $\langle h\rangle$, is defined following the work of Voth and Wang[50,51] as

$$\langle h\rangle = \frac{1}{N}\sum_i\sum_j\exp\left(-\frac{r_{ij}^2}{2\sigma^2}\right) \quad (3)$$

where r_{ij} is the distance, corrected for periodic boundary conditions, between two identical sites on different molecules, while σ is a scale length parameter given by $(1/\rho)^{1/3}$, with ρ being the number density of sites under consideration.

Conclusions

In this work, we have synthesized a series of 1-alkyl-3-methylpyridinium halides, trihalides and dichloroiodate compounds [C_nMP][X] with n = 12, 14, and 16 and the anion X being Cl^-, Br^-, I^-, Br_3^-, ICl_2^-, and I_3^-, in order to have a set of systems with a varying ratio between the cationic volume and the anionic volume. The thermotropic phase behavior was then studied by DSC and POM, where the phase and transition temperatures of the ILs are determined. Some conclusions that can be drawn from the results are that (i) for the ILs with the same alkyl chain length n, the melting and/or clearing point decreases as the atomic number of the halide anion increases; and (ii) for the ILs with the same anion, the melting and/or clearing point increases when increasing the chain length n. The smectic phase only occurs in the cases of N = 14 and 16 with a monoatomic halide anion. Since the cationic volume depends on n, it is apparent that the volume ratio of the cation to the anion significantly affects the appearance of the ionic smectic phase. More specifically, the ILs can have a stable smectic phase with a wide thermal range only when the volume ratio is above a constant value, as determined in ref. 33 for the imidazolium series.

The experimental results were rationalized with the aid of MD simulations performed on four systems with n = 12 and 16 and the anions X = Br^- and Br_3^-. The systems are heated gradually from the crystal phase until melting into the isotropic phase. The simulation results agree well, qualitatively, with the experimental results. In fact, for systems with the same n, those with the bromide anion have higher melting points than those with tribromide anions; for systems having the same anion, those with a larger n have higher melting points than the ones with a smaller n. Besides, for the simulated compounds, a stable smectic liquid crystal phase is observed only for [C_{16}MP][Br].

Based on the microscopic details obtained from the simulations, we propose an explanation for the volume effects on the phase behaviors: the larger chain length n leads to stronger vdW interactions stabilizing the thicker hydrophobic layers, and the more concentrated charge densities of the monoatomic halides stabilize the ionic layers by stronger electrostatic interactions. Both these effects stabilize the ionic smectic phase up to relatively high temperatures. In the opposite case with relatively short alkyl chains (therefore weak vdW interactions) and large anions (therefore weak electrostatic interactions) a liquid phase is stabilized, and we have ionic liquids stable at room temperature or even below that eventually crystallize into a solid crystal. As observed by Nelyubina for imidazolium-based ILCs,[33] there is a linear relationship between the volume (chain length) of the imidazolium cation and the volume of the anion where an ionic smectic phase appears. In this work, we have linked the cationic and anionic volumes with the energetic interactions of the nonpolar layer (mostly vdW) and polar layer (mostly electrostatic), respectively. Therefore, in order to answer the question we asked in the Introduction, why with larger anions a cation with a longer alkyl chain is needed in order to observe an ionic smectic phase, the answer is that the loss of electrostatic interactions in the ionic layer needs to be compensated by increased vdW interactions in the hydrophobic layer in order to keep the layered, yet fluid, structure in place.

Although the most common examples of ionic liquid crystal phases are based on alkylated nitrogen salts, therefore a

cationic head linked to an alkyl chain paired with some relatively small anion, there are interesting examples of oppositely charged systems, as mentioned in the Introduction, that is metal alkanoates.[35–38] It is noteworthy that our discussion is totally unrelated to the specific charge of the head of the ion containing the alkyl chain and the charge of the relatively smaller counterion. Therefore, our arguments apply equally well to the effect of increasing the size of the metal countercation in alkanoate salts and to the effect of increasing the size of the various counteranions in imidazolium or pyridinium salts.

The mechanism of the SmA-to-Isotropic clearing transition has also been investigated and we have highlighted the easier perturbation of the hydrophobic layer by the ionic layer when the anions have a lower charge density, which prevents the polar moiety of the cations and anions from penetrating through the thick hydrophobic layers. For these reasons, the ILs with a larger cation and a smaller anion, and thus a larger volume ratio between them, can have a more thermally stable crystal phase and exhibit a smectic phase only when the volume ratio is adequately large.

It should be noted that the above mechanism depends on the fact that the charge density of the anion correlates negatively with its volume, which is true for most anions. However, if an anion has the feature that the partial charges are unevenly distributed and weighted more on some parts of the anion than others, the correlation between the charge density and the volume of the anion is different and the above mechanism should be modified accordingly.

Finally, it is worth mentioning that quantitative agreement between simulations and experiments, concerning the transition temperatures, cannot be achieved in the present study. It is well-known that non-polarizable force fields, such as the one used here, overestimate the electrostatic interaction, resulting in an effective viscosity and molecular mobility lower than real systems at the same temperature.[64] On the other hand, no polarizable force fields are currently available for the IL systems we study in this work. A simple workaround that allows one to obtain nonetheless the correct structural features of the system is to run the simulation at a higher temperature in order to speed-up the sampling of the phase space, as we have done here.

Conflicts of interest

There are no conflicts to declare.

Acknowledgements

This work was supported by the National Natural Science Foundation of China (No. 11774357 and 11847612), and by the CNR-CAS 2017-2019 bilateral agreement as well as the CAS Biophysics Interdisciplinary Innovation Team Project (No. 2060299). The computations of this work were conducted on the HPC cluster of ITP-CAS and on the Tianhe-2 supercomputer. We thank Roberta Saini (DiSC, University of Padova) for help with the DSC measurements.

Notes and references

1 K. Goossens, K. Lava, C. W. Bielawski and K. Binnemans, *Chem. Rev.*, 2016, **116**, 4643–4807.
2 C. J. Bowlas, D. W. Bruce and K. R. Seddon, *Chem. Commun.*, 1996, 1625–1626.
3 Y. Nozaki, K. Yamaguchi, K. Tomida, N. Taniguchi, H. Hara, Y. Takikawa, K. Sadakane, K. Nakamura, T. Konishi and K. Fukao, *J. Phys. Chem. B*, 2016, **120**, 5291–5300.
4 A. Getsis and A.-V. Mudring, *Cryst. Res. Technol.*, 2008, **43**, 1187–1196.
5 W. Dobbs, B. Heinrich, C. Bourgogne, B. Donnio, E. Terazzi, M.-E. Bonnet, F. Stock, P. Erbacher, A.-L. Bolcato-Bellemin and L. Douce, *J. Am. Chem. Soc.*, 2009, **131**, 13338–13346.
6 M. R. Schenkel, J. B. Hooper, M. J. Moran, L. A. Robertson, D. Bedrov and D. L. Gin, *Liq. Cryst.*, 2014, **41**, 1668–1685.
7 W. Li, J. Zhang, B. Li, M. Zhang and L. Wu, *Chem. Commun.*, 2009, 5269–5271.
8 R.-T. Wang, G.-H. Lee and C. K. Lai, *CrystEngComm*, 2018, **20**, 2593–2607.
9 J. Tao, J. Zhong, P. Liu, S. Daniels and Z. Zeng, *J. Fluorine Chem.*, 2012, **144**, 73–78.
10 V. Causin and G. Saielli, *J. Mol. Liq.*, 2009, **145**, 41–47.
11 M. Bonchio, M. Carraro, G. Casella, V. Causin, F. Rastrelli and G. Saielli, *Phys. Chem. Chem. Phys.*, 2012, **14**, 2710–2717.
12 G. Casella, V. Causin, F. Rastrelli and G. Saielli, *Phys. Chem. Chem. Phys.*, 2014, **16**, 5048–5051.
13 V. Causin and G. Saielli, *J. Mater. Chem.*, 2009, **19**, 9153–9162.
14 P. K. Bhowmik, W. H. Xu and H. S. Han, *J. Polym. Sci., Part A: Polym. Chem.*, 1994, **32**, 3205–3209.
15 P. K. Bhowmik, H. S. Han, J. J. Cebe, R. A. Burchett, B. Acharya and S. Kumar, *Liq. Cryst.*, 2003, **30**, 1433–1440.
16 R.-T. Wang, G.-H. Lee and C. K. Lai, *J. Mater. Chem. C*, 2018, **6**, 9430–9444.
17 M. Butschies, M. Mansueto, J. C. Haenle, C. Schneck, S. Tussetschläger, F. Giesselmann and S. Laschat, *Liq. Cryst.*, 2014, **41**, 821–838.
18 M. Butschies, S. Sauer, E. Kessler, H.-U. Siehl, B. Claasen, P. Fischer, W. Frey and S. Laschat, *ChemPhysChem*, 2010, **11**, 3752–3765.
19 M. Butschies, W. Frey and S. Laschat, *Chem. – Eur. J.*, 2012, **18**, 3014–3022.
20 F. Yuan, S. Chi, S. Dong, X. Zou, S. Lv, L. Bao and J. Wang, *Electrochim. Acta*, 2019, **294**, 249–259.
21 D. Högberg, B. Soberats, R. Yatagai, S. Uchida, M. Yoshio, L. Kloo, H. Segawa and T. Kato, *Chem. Mater.*, 2016, **28**, 6493–6500.
22 R. Atasiei, M. Raicopol, C. Andronescu, A. Hanganu, A. L. Alexe-Ionescu and G. Barbero, *J. Mol. Liq.*, 2018, **267**, 81–88.
23 J. H. Lee, K. S. Han, J. S. Lee, A. S. Lee, S. K. Park, S. Y. Hong, J.-C. Lee, K. T. Mueller, S. M. Hong and C. M. Koo, *Adv. Mater.*, 2016, **28**, 9301–9307.

24 G. Saielli, *Crystals*, 2019, **9**, 274.
25 B. Ringstrand, H. Monobe and P. Kaszynski, *J. Mater. Chem.*, 2009, **19**, 4805–4812.
26 A. Pana, I. Pasuk, M. Micutz and V. Circu, *CrystEngComm*, 2016, **18**, 5066–5069.
27 K. Goossens, P. Nockemann, K. Driesen, B. Goderis, C. Goerller-Walrand, K. Van Hecke, L. Van Meervelt, E. Pouzet, K. Binnemans and T. Cardinaels, *Chem. Mater.*, 2008, **20**, 157–168.
28 X. Wang, L. Bai, S. Kong, Y. Song and F. Meng, *Liq. Cryst.*, 2018, **0**, 1–11.
29 S. Kondrat, M. Bier and L. Harnau, *J. Chem. Phys.*, 2010, **132**, 184901.
30 T. Margola, G. Saielli and K. Satoh, *Mol. Cryst. Liq. Cryst.*, 2017, **649**, 50–58.
31 G. Saielli, T. Margola and K. Satoh, *Soft Matter*, 2017, **13**, 5204–5213.
32 T. Margola, K. Satoh and G. Saielli, *Crystals*, 2018, **8**, 371.
33 Y. V. Nelyubina, A. S. Shaplov, E. I. Lozinskaya, M. I. Buzin and Y. S. Vygodskii, *J. Am. Chem. Soc.*, 2016, **138**, 10076–10079.
34 F. Xu, S. Matsubara, K. Matsumoto and R. Hagiwara, *J. Fluorine Chem.*, 2012, **135**, 344–349.
35 T. A. Mirnaya, V. D. Prisyazhnyi and V. A. Shcherbakov, *Russ. Chem. Rev.*, 1989, **58**, 1429–1450.
36 F. J. M. Casado, M. R. Riesco, M. I. R. Yélamos, A. S. Arenas and J. A. R. Cheda, *J. Therm. Anal. Calorim.*, 2012, **108**, 399–413.
37 T. A. Mirnaya and S. V. Volkov, in *Green industrial applications of ionic liquids*, ed. R. D. Rogers, K. R. Seddon and S. Volkov, Kluwer Academic Publisher, London, 2002, pp. 439–456.
38 G. Klimusheva, T. Mirnaya and Y. Garbovskiy, *Liq. Cryst. Rev.*, 2015, **3**, 28–57.
39 A. E. Bradley, C. Hardacre, J. D. Holbrey, S. Johnston, S. E. J. McMath and M. Nieuwenhuyzen, *Chem. Mater.*, 2002, **14**, 629–635.
40 V. P. Swamy, H. V. Thulasiram, F. Rastrelli and G. Saielli, *Phys. Chem. Chem. Phys.*, 2018, **20**, 11470–11480.
41 Y. Wang and G. A. Voth, *J. Am. Chem. Soc.*, 2005, **127**, 12192–12193.
42 J. N. A. Canongia Lopes and A. A. H. Pàdua, *J. Phys. Chem. B*, 2006, **110**, 3330–3335.
43 G. Saielli, A. Bagno and Y. Wang, *J. Phys. Chem. B*, 2015, **119**, 3829–3836.
44 W. Cao, Y. Wang and G. Saielli, *J. Phys. Chem. B*, 2018, **122**, 229–239.
45 W. Cao and Y. Wang, *Crystals*, 2019, **9**, 26.
46 G. Saielli, *Soft Matter*, 2012, **8**, 10279–10287.
47 Y. Ji, R. Shi, Y. Wang and G. Saielli, *J. Phys. Chem. B*, 2013, **117**, 1104–1109.
48 J. D. Holbrey and K. R. Seddon, *J. Chem. Soc., Dalton Trans.*, 1999, 2133–2140.
49 G. Saielli and Y. Wang, *J. Phys. Chem. B*, 2016, **120**, 9152–9160.
50 Y. Wang and G. A. Voth, *J. Phys. Chem. B*, 2006, **110**, 18601–18608.
51 Y. Wang and G. A. Voth, *J. Phys. Chem. B*, 2010, **114**, 8735–8743.
52 J. Wang, R. M. Wolf, J. W. Caldwell, P. A. Kollman and D. A. Case, *J. Comput. Chem.*, 2004, **25**, 1157–1174.
53 D. A. Case, I. Y. Ben-Shalom, S. R. Brozell, D. S. Cerutti, T. E. I. Cheatham, V. W. D. Cruzeiro, T. A. Darden, R. E. Duke, D. Ghoreishi, M. K. Gilson, H. Gohlke, A. W. Goetz, D. Greene, R. Harris, N. Homeyer, S. Izadi, A. Kovalenko, T. Kurtzman, T. S. Lee, S. LeGra, D. M. York and P. A. Kollman, *AMBER 2018*, University of California, San Francisco, 2018.
54 C. I. Bayly, P. Cieplak, W. Cornell and P. A. Kollman, *J. Phys. Chem.*, 1993, **97**, 10269–10280.
55 M. J. Frisch, G. W. Trucks, H. B. Schlegel, G. E. Scuseria, M. A. Robb, J. R. Cheeseman, G. Scalmani, V. Barone, B. Mennucci, G. A. Petersson, H. Nakatsuji, M. Caricato, X. Li, H. P. Hratchian, A. F. Izmaylov, J. Bloino, G. Zheng, J. L. Sonnenberg, M. Hada, M. Ehara, K. Toyota, R. Fukuda, J. Hasegawa, M. Ishida, T. Nakajima, Y. Honda, O. Kitao, H. Nakai, T. Vreven, J. A. M. Jr., J. E. Peralta, F. Ogliaro, M. Bearpark, J. J. Heyd, E. Brothers, K. N. Kudin, V. N. Staroverov, R. Kobayashi, J. Normand, K. Raghavachari, A. Rendell, J. C. Burant, S. S. Iyengar, J. Tomasi, M. Cossi, N. Rega, N. J. Millam, M. Klene, J. E. Knox, J. B. Cross, V. Bakken, C. Adamo, J. Jaramillo, R. Gomperts, R. E. Stratmann, O. Yazyev, A. J. Austin, R. Cammi, C. Pomelli, J. W. Ochterski, R. L. Martin, K. Morokuma, V. G. Zakrzewski, G. A. Voth, P. Salvador, J. J. Dannenberg, S. Dapprich, A. D. Daniels, Ö. Farkas, J. B. Foresman, J. V. Ortiz, J. Cioslowski and D. J. Fox, *Gaussian 09, Revision E.01*, Gaussian, Inc., Wallingford CT, 2009.
56 M. Parrinello and A. Rahman, *J. Appl. Phys.*, 1981, **52**, 7182–7190.
57 S. Nosé, *Mol. Phys.*, 1984, **52**, 255–268.
58 T. Darden, D. York and L. Pedersen, *J. Chem. Phys.*, 1993, **98**, 10089–10092.
59 W. Humphrey, A. Dalke and K. Schulten, *J. Mol. Graphics*, 1996, **14**, 33–38.
60 M. J. Abraham, T. Murtola, R. Schulz, S. Páll, J. C. Smith, B. Hess and E. Lindahl, *SoftwareX*, 2015, **1–2**, 19–25.
61 D. K. Jordan, J. A. Kitchen, D. Y. Hegh, S. Brooker and E. W. Tan, *Acta Crystallogr., Sect. E: Struct. Rep. Online*, 2008, **64**, o2457.
62 G. V. Shilov, O. N. Kazheva, O. A. D'yachenko, M. S. Chernov'yants, S. S. Simonyan, V. E. Gol'eva and A. I. Pyshchev, *Russ. J. Phys. Chem. A*, 2002, **76**, 1295–1301.
63 M. A. Bates and G. R. Luckhurst, *J. Chem. Phys.*, 1999, **110**, 7087–7108.
64 F. Dommert, K. Wendler, R. Berger, L. D. Site and C. Holm, *ChemPhysChem*, 2012, **13**, 1625–1637.